ELSEVIER

Journal of Organometallic Chemistry 528 (1997) 163–178

Journal of Organometallic Chemistry

Platinum(I) dimers and platinum(0) triangles with polyaromatic phosphine ligands [1]

Thomas E. Müller, Florent Ingold, Stefan Menzer, D. Michael P. Mingos *, David J. Williams

Department of Chemistry, Imperial College of Science, Technology and Medicine, London SW7 2AY, UK

Received 10 May 1996; accepted 30 May 1996

Abstract

The metal–metal bonded platinum(I) dimers $[Pt_2Cl_2(CO)_2(PR_3)_2]$ ($PR_3 = PNpPh_2$ and PFc_2Ph; Np = naphthyl, Fc = ferrocenyl) have been synthesised by reduction of the monometallic precursor $[PtCl_2(COD)]$ in the presence of CO and the appropriate phosphine. $^{31}P\{^1H\}$ NMR studies have indicated the presence of a fluxional process which renders the two halves of this type of platinum dimer equivalent on the NMR timescale. Suggestions for a possible mechanism for this process are made on the basis of extended Hückel calculations. Slight variation of the reaction conditions lead to the isolation of the *triangulo*- cluster compounds $[Pt_3(\mu\text{-}CO)_3(PR_3)_3]$ ($PR_3 = PNpPh_2$ and PNp_2Ph).

Keywords: Platinum; Fluxionality; Platinum clusters; Platinum(I) dimers; Extended Hückel calculations; Polyaromatic phosphines

1. Introduction

Recently we have described the synthesis and properties of complexes of polyaromatic phosphine ligands containing combinations of naphthyl (Np), anthracenyl (An) and ferrocenyl (Fc) substituents [1]. These complexes have shown interesting properties [2] and, for example, have led to the definition of novel T-shaped hydrogen bonds between the proton of $CHCl_3$ and the triple bond in $R_3P\text{–}Au\text{–}C{\equiv}C\text{–}Au\text{–}PR_3$ ($PR_3 = PNpPh_2$, PNp_2Ph) [3]. The Tolman cone angles [4] and the gas phase ionisation potentials [5] of these ligands have also been investigated, and their bonding ability to platinum(II) complexes established [6]. In this paper, the synthesis and characterisation of metal–metal bonded compounds of platinum stabilised by these ligands are described.

The *triangulo*- cluster compounds of platinum $[Pt_3(CO)_3(PR_3)_3]$ and $[Pt_3(CO)_3(PR_3)_4]$ have been known for more than 20 years, and the synthetic routes to them are well documented [7]. The chemistry of platinum dimers, where the platinum–platinum bond is supported by bridging ligands, has also been established [8]. There are also examples of dinuclear unbridged platinum(I) compounds. These can be stabilised by phosphine, carbonyl, isocyanide and related ligands and the basic types of complex and their structures are illustrated in Scheme 1. With the exception of the cyclopentadienyl complex, they have square-planar geometries about the platinum atoms and approximately staggered geometries with respect to the platinum–platinum bond. The dihedral angle between the square-planes varies from 88° to 60°.

The compounds of particular interest in the context of the current paper are $[Pt_2Cl_2(CO)_2(PR_3)_2]$ (Type I in Scheme 1), which have been synthesised from oxidation of the *triangulo*- cluster $[Pt_3(\mu\text{-}CO)_3(PR_3)_3]$ with 1.5 mol Cl_2, elimination of H_2 from $[PtHCl(CO)(PR_3)]$ [9] and addition of phosphines to $[Pt_2Cl_4(CO)_2]^{2-}$ [10]. The latter dinuclear platinum(I) compound is readily obtained by a photolytic reaction from K_2PtCl_4 in HCl_{aq} in the presence of CO [11]. In a similar reaction, K_2PtCl_4 reacts in aqueous solution in the presence of CNMe to give $[Pt_2(CNMe)_6]^{2+}$ [12]. The proposed mechanism involves coordination of the isonitrile, followed by a nucleophilic attack of water at the coordinated isonitrile, initiating the reduction of the platinum. In a very similar reduction process the compound $[Pt_2(CO)_2(P\text{–}P)_2]^{2+}$ (P–P = bidentate tertiary phos-

* Corresponding author.

[1] Dedicated to Professor Malcolm Green FRS on the occasion of his 60th birthday.

PII S0022-328X(96)06547-3

Platinum(I) Dimer	Phosphine	L	Reference
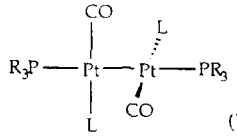 (Type I)	P^tBu_2Ph	Cl	[9]
	PPh_3	Cl	[10]
	PPh_3	C_6F_5	[18]
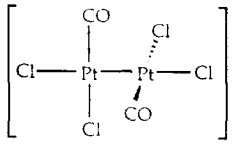 $[^nPr_4N]_2$			[11,56]
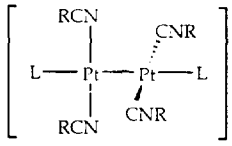 $[PF_6]_2$	L = CNR = CNMe		[12,10]
$[PF_6]_2$	L = PPh_3, R = Xyl		[17]
no Anion	R = 2,4-^{t}Bu$_2$-6-MeC$_6$H$_2$	Cl	[14]
no Anion	R = 2,4,6-^{t}Bu$_3$C$_6$H$_2$	Cl	[14]
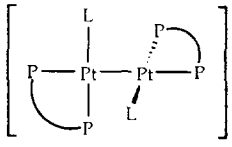 $[PF_6]_2$	$Ph_2P(CH)_2PPh_2$	CNXyl, CNMes	[15]
$[PF_6]_2$	$Ph_2P(CH_2)_nPPh_2$, n=2-4	CNXyl, CNMes	[15]
$[PF_6]_2$	$Ph_2P(CH_2)_2PPh_2$	CO	[13]
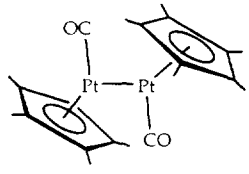			[16]
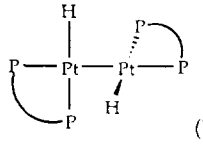 (Type II)	$^tBu_2P(CH_2)_2P^tBu_2$		[19]
	$^iPr_2P(CH_2)_2P^iPr_2$		[19]
	$Cy_2P(CH_2)_2PCy_2$		[19]

^{t}Bu = *tert*-butyl, C_6F_5 = pentafluorophenyl, ^{n}Pr = *n*-propyl, Xyl = xylyl, Mes = mesityl, ^{i}Pr = *iso*-propyl, Cy = cyclohexyl

Scheme 1. Unbridged dimeric platinum(I) complexes.

phine) was obtained from $[Pt(H_2O)_2(P-P)]^{2+}$ and CO [13]. The dimers $[Pt_2Cl_2(CNR)_4]$ have been obtained by the electrolytic reduction of $[PtCl_2(CNR)_2]$ [14], which were then reacted with tertiary diphosphines to give $[Pt_2(CNR)_2(P-P)_2]^{2+}$. The latter dimers can also be obtained directly from the electrolytic reduction of $[Pt(CNR)_2(P-P)]^{2+}$ [15]. In the dimer $[Pt_2Cp^*_2(CO)_2]$, the pentamethylcyclopentadienyl group (Cp^*) effectively replaces two ligands. It has been obtained by the reaction of $[PtCl_3(CO)]^-$ with Cp^*MgCl [16]. A conproportionation between platinum(II) and platinum(0) provides an alternative route into platinum(I) chemistry, and has resulted in the isolation of $[Pt_2(CNR)_4(PPh_3)_2]^{2+}$ [17] and $[Pt_2(CO)_2(C_6F_5)_2(PPh_3)_2]$ [18]. Most recently, the elimination of hydrogen from $[PtH_2(P-P)]$ has been used for the synthesis of $[Pt_2H_2(P-P)_2]$ [19].

2. Results and discussion

2.1. Synthesis

$[PtCl_2(COD)]$ (COD = cyclooctadiene) was used as the starting material for the investigation of the reactivities of the polyaromatic phosphine ligands, and the results are summarised in Scheme 2. $[PtCl_2(COD)]$ was dissolved in $CHCl_3$, 1 mol equivalent of $PNpPh_2$, PAn_2Ph or PFc_2Ph was added and the solution saturated with CO. After cooling to about −50 °C, 2 mol

equivalents of $LiBHEt_3$ were added. The solutions were warmed slowly and the reaction was monitored by $^{31}P\{^1H\}$ NMR, which indicated the formation of a dimeric species in approximately 40% yield and several mononuclear platinum compounds. Chromatographic separation of the mixture yielded pure crystalline samples of yellow $[Pt_2Cl_2(CO)_2(PNpPh_2)_2]$ (**1a**) or orange $[Pt_2Cl_2(CO)_2(PFc_2Ph)_2]$ (**1b**). The latter was characterised by an X-ray structural determination. $[Pt_2Cl_2(CO)_2(PAn_2Ph)_2]$ (**1c**) was observed in the $^{31}P\{^1H\}$ NMR spectrum, but proved to be less stable and decomposed upon warming to ambient temperatures. From the reaction mixture of **1b**, one of several side products was isolated and identified as *trans*-$[PtClH(PFc_2Ph)_2]$.

When $[PtCl_2(COD)]$ was dissolved in $CHCl_3$ and CO and the phosphines $PNpPh_2$ and PNp_2Ph were added at room temperature, the mononuclear compounds $[PtCl_2(CO)(PNpPh_2)]$ (**2a**) and $[PtCl_2(CO)(PNp_2Ph)]$ (**2b**) were isolated as white solids. Subsequent reduction of **2a** and **2b** with Zn in THF led to the formation of dark green solutions which gradually (one day) turned dark red. After recrystallisation and chromatographic separation (for the PNp_2Ph complex), the *triangulo*-clusters $[Pt_3(\mu\text{-}CO)_3(PNpPh_2)_3]$ (**3a**) and $[Pt_3(\mu\text{-}CO)_3(PNp_2Ph)_3]$ (**3b**) were isolated as red crystalline solids. The compound **3b** is significantly less stable than **3a**, and gradually decomposes in solution at room

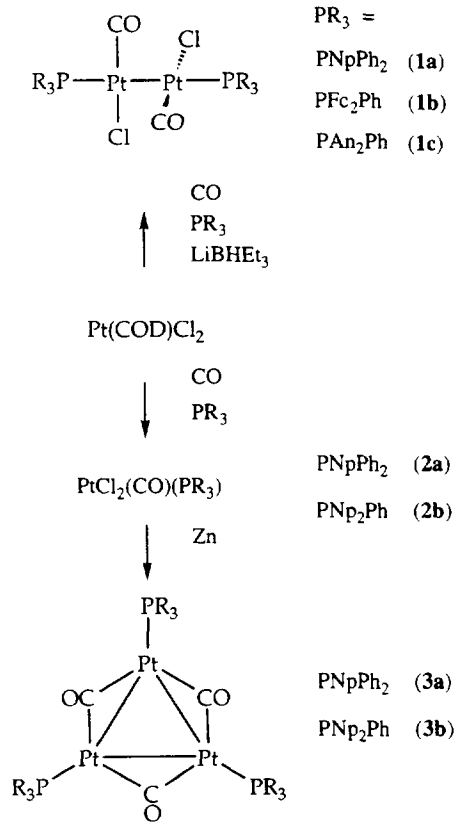

Scheme 2. Routes used for the synthesis of platinum(I) dimers and platinum(0) triangles with polyaromatic phosphine ligands.

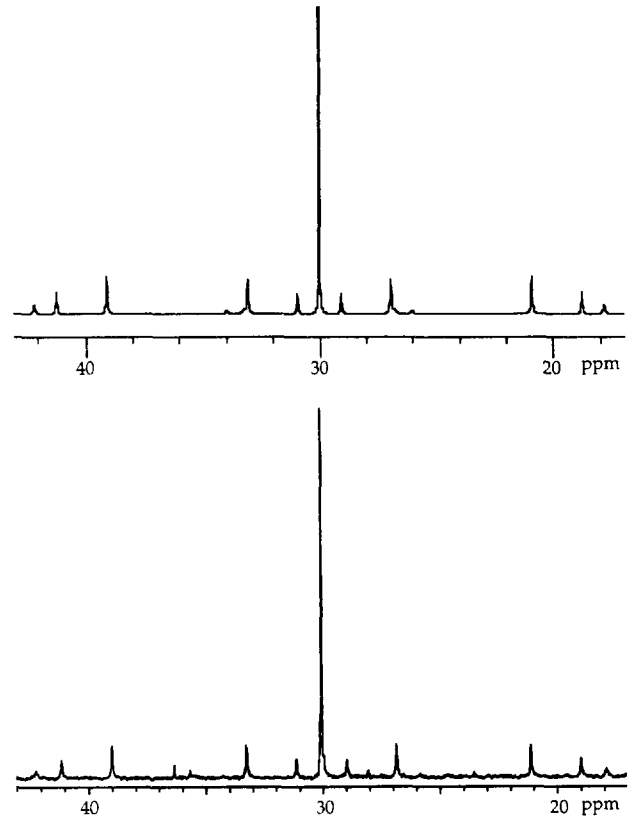

Fig. 1. Simulated and observed $^{31}P\{^1H\}$ spectrum of the complex $[Pt_2Cl_2(CO)_2(PNpPh_2)]$ (**1a**).

temperature. It is clear from these results that the increasing steric requirements of the polyaromatic phosphine ligands are influencing the yields and stabilities of the resulting binuclear and trinuclear compounds.

2.2. Spectroscopic characterisation

The IR spectrum of **1a** shows two strong bands at 2036 and 2052 cm^{-1}, indicating terminally bound CO groups. For complex **1b** these absorptions are shifted to slightly lower wavelengths (2018 and 2032 cm^{-1}). Absorptions due to ν(Pt–Cl) were observed at 322 cm^{-1} for **1a** and 327 cm^{-1} for **1b**. Raman spectroscopy shows the bands due to ν(Pt–Pt) at 193 cm^{-1} for **1a** and 190 cm^{-1} for **1b**. This is in accordance with ν(Pt–Pt) = 171 cm^{-1} for $[Pt_2Cl_4(CO)_2][^nPr_4N]_2$ [5].

The $^{31}P\{^1H\}$ NMR spectra of **1a** and **1b** (Fig. 1 for **1a**) show a single resonance at 30.0 and 26.5 ppm respectively. The satellites are characteristic of two chemically equivalent phosphine environments in a dinuclear complex with a linear R_3P–Pt–Pt–PR_3 arrangement [17]. The spectrum is a superposition of the subspectra related to the three isotopomers Pt–Pt (44.4% abundance), ^{195}Pt–Pt (44.4% abundance) and ^{195}Pt–^{195}Pt (11.1% abundance). A computer simulation using the program GeNMR [20] has confirmed the assignment of the coupling constants (Fig. 1 for **1a**). The ^{195}Pt

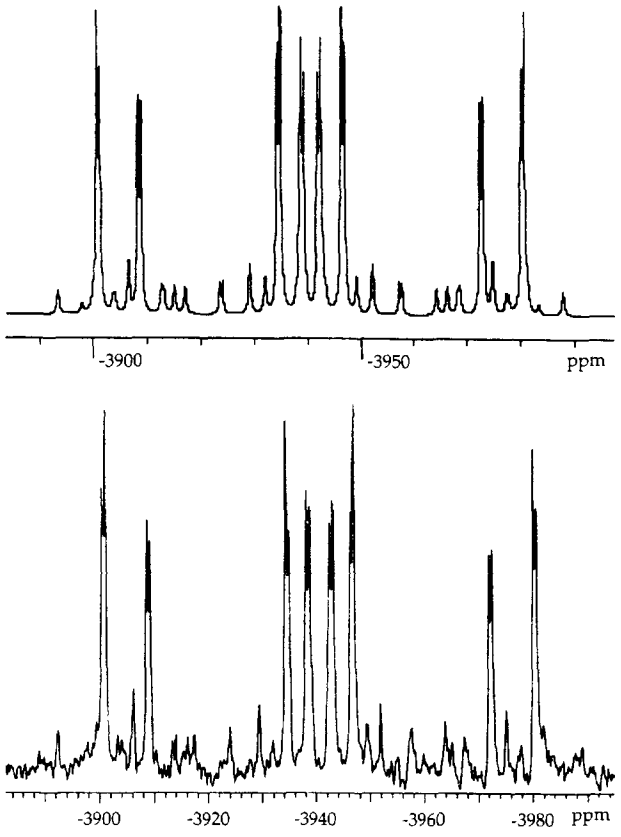

Fig. 2. Simulated and observed ^{195}Pt spectrum of $[Pt_2Cl_2(^{13}CO)_2(PNpPh_2)_2]$ (**1a**).

NMR spectrum shows a doublet of doublets centred at −3940 ppm and −3969 ppm for **1a** and **1b** respectively, which is due to the $R_3P-^{195}Pt-Pt-PR_3$ isotopomer. A ^{13}C enriched (100%) sample of $[Pt_2Cl_2(^{13}CO)_2(PNpPh_2)_2]$ shows 16 lines of approximately equal intensity centred at −3940 ppm, the pattern being due to one bond and two bond coupling to the ^{13}C and ^{31}P nuclei (Fig. 2). The low intensity signals arise from the subspectrum for $R_3P-^{195}Pt-^{195}Pt-PR_3$ and allow an estimation of the $^{195}Pt-^{195}Pt$ coupling constant as ca. 748 Hz. This compares closely with the value of 760 Hz measured for $[Pt_2Cl_2(CO)_2(PPh_3)_2]$ [10]. The spectroscopic data indicate the assignment of the structure as Type I (Scheme 1), but to confirm the structure unambiguously an X-ray crystal structural determination on $[Pt_2Cl_2(CO)_2(PFcPh_2)_2]$ (**1b**) was undertaken and the results are shown in Fig. 3.

The IR spectra of compounds **3a** and **3b** show strong absorptions for $\nu(C{\equiv}O)$ at 1795 and 1793 cm^{-1} respectively, indicating the bridging nature of the carbonyl ligands. The $^{31}P\{^1H\}$ NMR spectra of **3a** and **3b** (Fig. 4 for **3a**) show a single resonance at 50.6 and 48.3 ppm respectively, with satellites arising from the ^{195}Pt isotopomers. The pattern is characteristic of a symmetrically substituted platinum triangle [21,22], and the assignment of the coupling constants has been confirmed via a computer simulation (Fig. 4). From the low intensity signals due to $R_3P-^{195}Pt-^{195}Pt-PR_3$, the $^1J(^{195}Pt,$

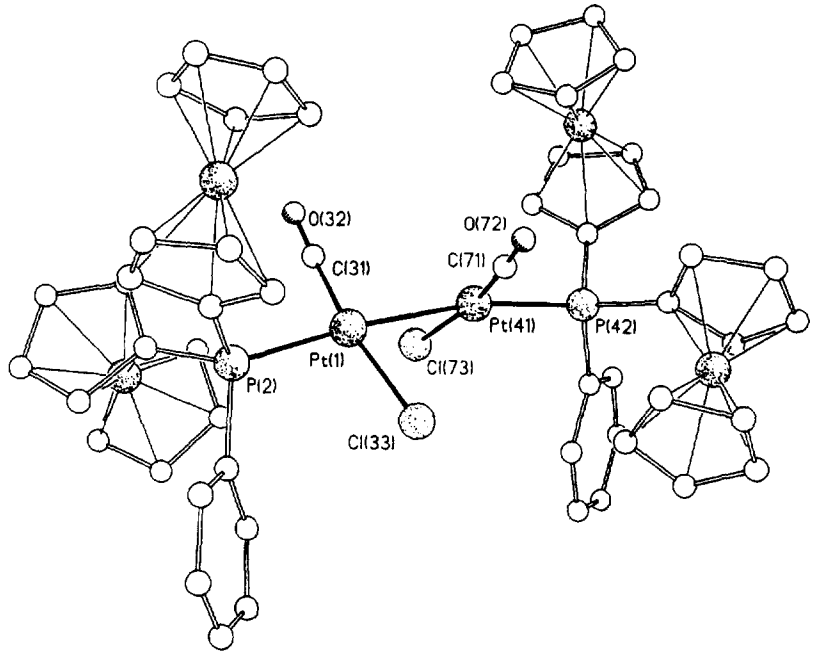

Fig. 3. Molecular structure and numbering scheme of (**1b**). Selected bond lengths (Å) and angles (°): Pt(1)–Pt(41) = 2.6267(8), Pt(1)–P(2) = 2.325(3), Pt(41)–P(42) = 2.344(3), Pt(1)–Cl(33) = 2.306(4), Pt(41)–Cl(73) = 2.313(4), Pt(1)–C(31) = 1.84(2), Pt(41)–C(71) = 1.81(2), C(31)–O(32) = 1.11(2), C(71)–O(72) = 1.13(2), Pt(41)–Pt(1)–P(2) = 175.1(1), Pt(1)–Pt(41)–P(42) = 170.0(1), Pt(41)–Pt(1)–Cl(33) = 87.4(1), Pt(1)–Pt(41)–Cl(72) = 88.9(1), Pt(41)–Pt(1)–C(31) = 83.7(5), Pt(1)–Pt(41)–C(71) = 81.9(5), Pt(1)–C(31)–O(32) = 176(2), Pt(42)–C(71)–O(72) = 175(2).

^{195}Pt) coupling constant could be estimated as 1805 Hz. The ^{195}Pt spectrum of compound **3a** shows a triplet of doublets centred at −4536 ppm (Fig. 5). The spectrum was satisfactorily simulated.

2.3. Crystal structural analysis of $[Pt_2Cl_2(CO)_2(PFc_2Ph)_2]$ (1b)

Complex **1b** consists of two square-planar $PtCl(CO)(PFc_2Ph)$ units bonded via a direct metal–metal bond unsupported by any bridging ligand (Fig. 3). The two principal coordination planes are both close to planarity (mean deviation 0.064 Å for Pt(1), P(2), Cl(33), C(31), O(32) and 0.023 Å for Pt(41), P(42), Cl(73), C(71), O(72)). The planes are oriented approximately perpendicular to each other, with a dihedral angle of 65.6°. This arrangement renders the complex chiral. The compound crystallises in the centrosymmetric space group $C2/c$, and thus equal numbers of both isomers are present in the crystal. A comparison with structures of other unbridged platinum(I) dimers shows that dihedral angles are generally between 60° and 88° (Table 1). A dihedral angle of 90° would minimise the steric repulsion between the ligands on adjacent platinum atoms. In contrast to this a 45° angle would enable the interaxial filled d-orbitals to be as remote from one another as possible, minimising the antibonding interaction between them. As a consequence, π-donor ligands, e.g. Cl, appear to favour smaller dihedral angles, close to 60°, while π-acceptor ligands, such as C≡N, favour larger dihedral angles, close to 90°.

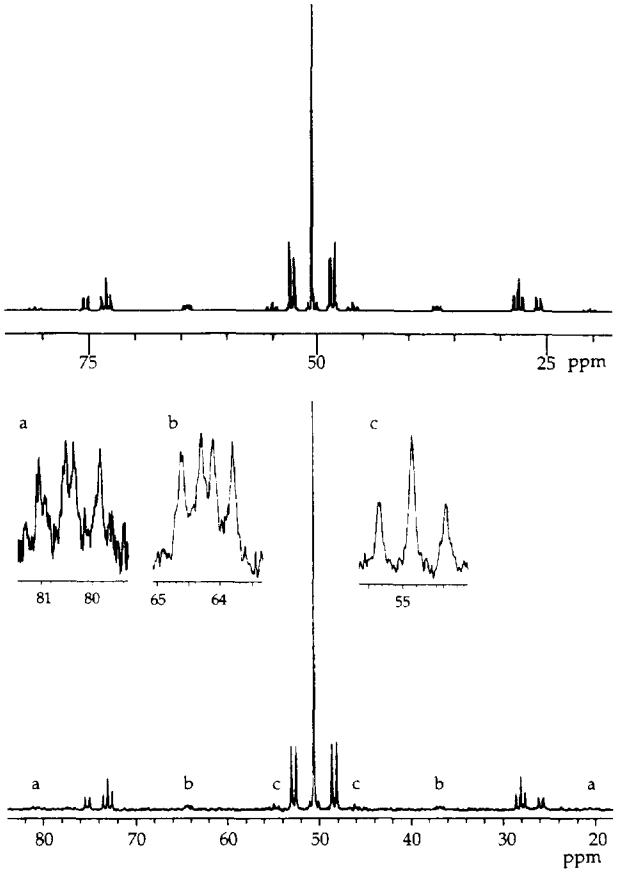

Fig. 4. Simulated and observed $^{31}P\{^1H\}$ spectrum of $[Pt_3(CO)_3(PNpPh_2)_3]$ (**3a**).

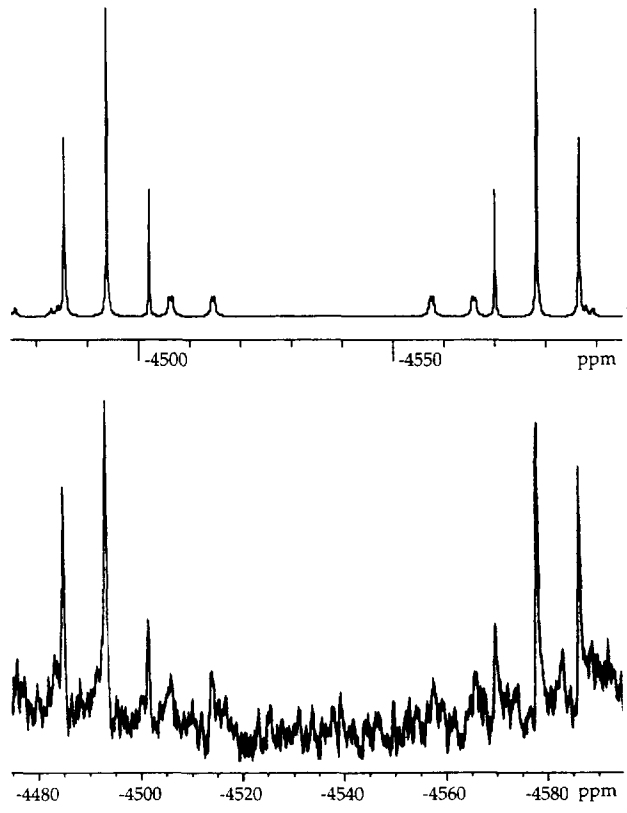

Fig. 5. Simulated and observed ^{195}Pt spectrum of $[Pt_3(CO)_3(PNpPh_2)_3]$ (**3a**).

The Pt(1)–Pt(2) separation of 2.627(1) Å for **1b** is consistent with a direct Pt(I)–Pt(I) bond and is within the range (2.56–2.65 Å) found in Pt(I) dimers containing an unsupported Pt–Pt bond (Table 1). The table also provides comparisons with dimers which have different oxidation states of platinum. The unbridged platinum(0) complex (**a**) shows a longer Pt–Pt separation of 2.77 Å [23]. In square-planar platinum(II) complexes intermolecular Pt–Pt distances of more than 3.1 Å are commonly observed [24], and for complexes **k**–**n** distances below ca. 3.4 Å have been interpreted in terms of weak metal–metal interactions. A theoretical study on the weakly bonding nature of M · · · M contacts between square-planar ML_4-d_8 molecules has recently been published [25]. The platinum(III) complexes **o** and **p** are based on two octahedral platinum environments bound via a Pt–Pt bond. The bond separation (2.69–2.70 Å) is only slightly larger than that in the Pt(I) dimers. There is one example, **q**, where a tetragonal pyramidal platinum complex [26] forms discrete dimers in the solid state with a Pt–Pt separation of 2.75 Å, but it is difficult

to assign where the electrons reside and the oxidation state remains ambiguous [27]. Generally, platinum(I) dimers show significantly shorter Pt–Pt separations than dimers with different oxidation states of platinum.

The structure of **1b** is closely related to $[Pt_2Cl_2(CO)_2(P^tBu_2Ph)_2]$ [9]. Although the overall appearance is comparable, small differences in the bond lengths and angles are observed which can largely be attributed to the different steric and electronic properties of the phosphine ligand. It is noteworthy that the central P–Pt–Pt–P unit is curved (Pt(1)–Pt(41)–P(42) = 170.0(1)°, Pt(41)–Pt(1)–P(2) = 175.1(1)°). The CO, and to a lesser extent the Cl, ligands bend away from the phosphine, avoiding intramolecular steric conflicts with the large ferrocene groups (Pt(1)–Pt(41)–C(71) = 81.9(5)°, Pt(41)–Pt(1)–C(31) = 83.7(5)°, Pt(1)–Pt(41)–Cl(73) = 88.9(1)°, Pt(41)–Pt(1)–Cl(33) = 87.4(1)°).

2.4. Fluxional processes

Fluxional processes based on mutual rotation of the coordination planes have been observed in the platinum(0) complex $[Pt_2(P–P)_2]$ (P–P = $^tBu_2P(CH_2)_3P^tBu_2$) [23]. EH calculations indicated that there was no significant barrier (3.8 kJ mol^{-1}) for a rotation about the Pt–Pt bond [28]. It was predicted that electron transfer out of the π_d^* orbital, which would effectively result in a Pt(I) dimer, would lead to a substantially higher rotational barrier (50.6 kJ mol^{-1}). In subsequent variable temperature NMR experiments on $[Pt_2H_2(P–P)_2]$, the coalescence temperature for a fluxional process was measured as −36 °C, −54 °C and less than −90 °C for P–P = dcype, dippe and dtbpe respectively [19]. For $[Pt_2Cp^*_2(CO)_2]$, a limiting temperature below −90 °C has been observed [16]. The energy barrier which can be estimated from this experiment using the Gutowsky equation [29] ($\Delta J > 0$ Hz) is very low ($\Delta G^{\#} <$ 31.0 kJ mol^{-1}), but a precise value was not reported. In these complexes the fluxional process is more complicated and the suggested mechanism involves not only rotation around the Pt–Pt bond but also intramolecular exchange of H or CO. Extended Hückel (EH) calculations have been performed on the model compounds $[Pt_2Cl_2(CO)_2(PH_3)_2]$ [9] and $[Pt_2Cl_2(CNH)_4]$ [14], which suggest rotation about the Pt–Pt bond to be a high energy process (222 kJ mol^{-1} and 357 kJ mol^{-1} respectively). These values may be reduced by optimisation of the Pt–Pt bond distances and the Pt–Pt–L angles (125 kJ mol^{-1} and 203 kJ mol^{-1} respectively), but the calculated barrier of the process remains high.

The large variation between the reported and calculated barriers in these platinum compounds led us to investigate the low temperature behaviour of dimer **1a**. The $^{31}P\{^1H\}$ NMR of **1a** in CD_2Cl_2 shows one signal at 30.0 ppm which continuously broadens when the temperature is lowered. A limiting temperature could not be reached upon cooling to −95 °C, which corresponds to an activation energy of less than 45 kJ mol^{-1}. Platinum

Table 1
Structurally characterised unbridged platinum dimers

Complex		Oxidation state	d(Pt–Pt) (Å)	Dihedral angle (°)	Reference
$[Pt_2(dtbpp)_2]$	**a**	0	2.765(1)	82	[23]
$[Pt_2Cl_2(CO)_2(PFc_2Ph)_2]$	**b**	I	2.627(1)	66	this work
$[Pt_2Cl_2(CN^tBu_2MeC_6H_2)_4]$	**c**	I	2.563(2), 2.561(2)	88	[14]
$[Pt_2H_2(dippe)_2]$	**d**	I	2.578(1)	87	[19]
$[Pt_2Cl_4(CO)_2][^nPr_4N]_2$	**e**	I	2.584(2)	60	[23]
$[Pt_2(C_6F_5)_2(CO)_2(PPh_3)_2]$	**f**	I	2.599(1)	79	[18]
$[Pt_2Cl_2(dtbpe)_2]$	**g**	I	2.609(1)	ca. 72	[19]
$[Pt_2Cl_2(CO)_2(P^tBu_2Ph)_2]$	**h**	I	2.628(1)	70	[9]
$[Pt_2(CO)_2(C_5Me_5)_2]$	**i**	I	2.636(1)	74	[16]
$[Pt_2(dppp)_2(CNMes)_2]$[a]	**j**	I	2.653(1)	85	[15]
$[Pt_2Cl_4(NHCOH^tBu)_4]$	**k**	II	3.165(1)		[44]
$[Pt_2(dpp)_2(CH_3CN)_2](ClO_4)_2$	**l**	II	3.37		[57]
$[Pt_2(N_2C_3H_4)_4(N_2C_3H_3)_4]$	**m**	II	3.370		[58]
$[Pt_2Cl_4(NHCOH^tBu)_4]$	**n**	II	3.399(1)		[44]
$[Pt_2Cl_6(NHCOH^tBu)_4]$	**o**	III	2.694(1)		[59]
$[Pt_2Cl_2(C_8H_{12}(=NO)_2H)_4]$	**p**	III	2.696(1)		[60]
$[Pt_2(S_2C_2H_2)_4]$	**q**	unknown	2.748(2)		[26]

[a] From EXAFS: $[Pt_2(dppen)_2(XylNC)_2]$, d(Pt–Pt) = 2.653(8) Å; $[Pt_2(dppe)_2(XylNC)_2]$, d(Pt–Pt) = 2.635(8) Å; $[Pt_2(dppp)_2(XylNC)_2]$, d(Pt–Pt) = 2.648(8) Å; $[Pt_2(dppb)_2(XylNC)_2]$, d(Pt–Pt) = 2.625(8) Å.

dtbpp = 1,3-bis(ditert-butylphosphino)prospan, $CN^tBu_2MeC_6H_2$ = 2,4-ditert-butyl-6-tolyl, dippe = 1,2-bis(diisopropylhossphino)ethane, C_6F_5 = pentafluorophenyl, dtbpe = 1,2-bis(ditert-butylphosphino)ethane, C_5Me_5 = pentamethylcyclopentadienyl, dppp = 1,3-bis(diphenylphosphino)propane, $NHCOH^tBu$ = 1-hydroxyneopentylideneamido, dpp = 2,9-diphenyl-1,10-phenanthroline-4′-yl, $N_2C_3H_4$ = dipyrazole, $N_2C_3H_3$ = dipyrazolato, $C_8H_{12}(=NO)_2H$ = cyclocta-α-dioximato, $S_2C_2H_2$ = bis(ethylene-1,2-dithiolene), dppen = *cis*-1,2-bis(diphenylphosphino)ethene, dppe = 1,2-bis(diphenylphosphino)ethane, dppb = 1,4-bis(diphenylphosphino)butane.

dimers of Type I have C_2 symmetry and should remain chiral in solution if the rotational barrier about the Pt–Pt bond and the activation energy for the interchange of carbonyls are large. It should therefore be possible to distinguish the enantiomers in the NMR spectra using a chiral solvating agent. Intermolecular diastereomeric interactions occur, which make the two enantiomers chemically different. However, if stereomutation between the two enantiomers is fast at room temperature, the NMR spectra of the two isomers will be indistinguishable. If these spectra are obtained at a sufficiently low temperature, it may be possible to make the interconversion rate slow on the NMR timescale. Different spectra will be obtained in a chiral environment for the R and S conformational enantiomers. This effect has been used mainly in organic chemistry to distinguish between the enantiomers [30–32] and to determine energy barriers [31,33,34] and has been described in some detail in a recent review [35].

Table 2
Variable temperature $^{13}C\{^1H\}$ NMR data for the carbonyl groups in $[Pt_2Cl_2(^{13}CO)_2(PNpPH_2)_2]$ in CD_2Cl_2

Temperature (°C)	δ (ppm)	$^1J(^{13}C,^{195}Pt)$ (Hz)	$^2J(^{13}C,^{195}Pt)$ (Hz)
−95	168.3	1978.7	—
−60	168.4	1966.6	—
−20	168.6	1962.8	—
+20	168.8	1959.3	29.0

The variable temperature experiments on **1a** were repeated in the presence of a large excess of (1R)-(+)-camphor. Camphor weakly coordinates to platinum, which enhances the diastereomeric interaction. Cam-

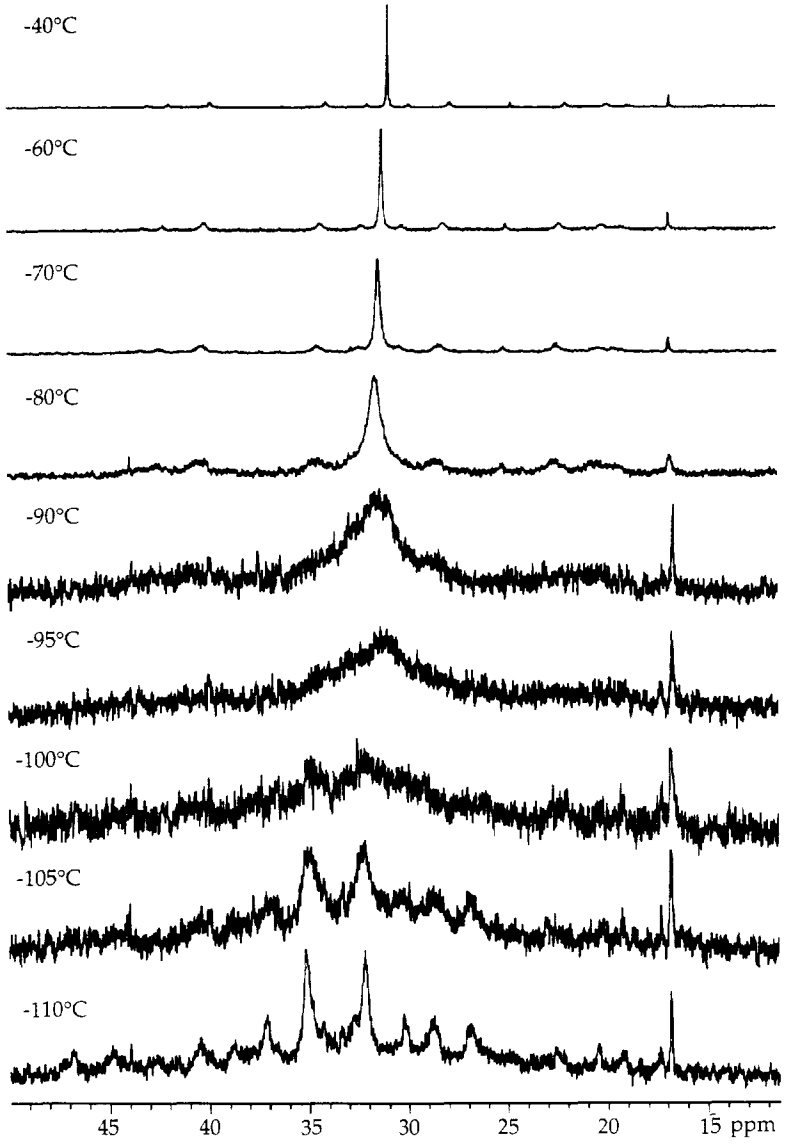

Fig. 6. Variable temperature $^{31}P\{^1H\}$ NMR spectrum of (**1a**) in the presence of (1R)-(+)-camphor.

Table 3
Variable temperature ^{195}Pt NMR data for $[Pt_2Cl_2(^{13}CO)_2(PNpPh_2)_2]$ in CD_2Cl_2

Temperature (°C)	δ (ppm)	$^1J(^{195}Pt,^{13}C)$ (Hz)	$^2J(^{195}Pt,^{13}C)$ (Hz)	$^1J(^{195}Pt,^{31}P)$ (Hz)	$^2J(^{195}Pt,^{31}P)$ (Hz)
−60	broadening				
−40	−3944	1964.7	21.0	2183.6	452.5
−20	−3943	1962.6	31.6	2183.6	457.8
0	−3942	1962.6	31.6	2183.6	463.0
+20	−3940	1957.3	31.6	2196.8	473.5

phor has the additional advantage that it reduces the freezing point of CD_2Cl_2. The $^{31}P\{^1H\}$ variable temperature NMR of **1a** (12 mg **1a** and 150 mg (1R)-(+)-camphor in 0.5 cm^{-3} CD_2Cl_2) shows a broadening of the signal at 30.0 ppm upon cooling which is accompanied by a shift of the resonance towards lower fields (Fig. 6). At −90 °C a shoulder appears which resolves at −110 °C into two signals at 32.1 and 35.1 ppm. The coalescence temperature was estimated at −98 ± 10 °C. Using the Gutowsky equation [29] this corresponds to an activation energy of $\Delta G^{\#} = 32.5 \pm 1.6$ kJ mol^{-1}. Clearly a low temperature process is present which renders the two enantiomers of the platinum dimer equivalent in the $^{31}P\{^1H\}$ NMR spectrum at room temperature.

The complexation and diastereomeric interaction between **1a** and camphor could lead to a change in the rate of the fluxional process. The inversion of the chirality can occur in the free and in the associated complex. The question of how this influences the energy measured has been addressed by organic chemists. Generally, it is found that coordination leads to little change in the exchange rate [31,33,34]. Therefore, the 32.5 kJ mol^{-1} barrier may be taken as an estimate for the fluxional process which renders the two sides of the dimer NMR equivalent. In order to rationalise the exchange process the synthesis of **1a** was repeated using ^{13}CO.

No differences between the $[Pt_2Cl_2(^{13}CO)_2(PNpPh_2)_2]$ compound and the unenriched compound were detected in the $^{31}P\{^1H\}$ variable temperature NMR spectra. However, upon lowering the temperature the $^{13}C\{^1H\}$ signal due to the carbonyl carbons shows a shift towards high field from 168.8 to 168.3 ppm (Table 2). The coupling constant $^1J(^{13}C,^{195}Pt)$ increases, while $^2J(^{13}C,^{195}Pt)$ decreases. The satellites due to the ^{195}Pt–^{195}Pt isotopomer, which are clearly visible at room temperature, disappear upon lowering the temperature. The ^{195}Pt signal shifts from −3940 ppm at +20 °C to −3944 ppm at −40 °C (Table 3). $^1J(^{195}Pt,^{13}C)$ and $^1J(^{195}Pt,^{31}P)$ show only little change when the temperature is varied. However, $^2J(^{195}Pt,^{13}C)$ decreases from 31.6 Hz at +20 °C to 21.0 Hz at −40 °C and $^2J(^{195}Pt,^{31}P)$ decreases from 473.5 Hz at +20 °C to 452.5 Hz at −40 °C. The observed changes in chemical shift and in the coupling constants are consistent with a fluxional process present in $[Pt_2Cl_2(^{13}CO)_2(PNpPh_2)_2]$. Intermediate spectra where the signals are broadened could not be observed in the ^{13}C and ^{195}Pt spectra as the compound decomposes when the temperature is raised above room temperature. For these nuclei the exchange between the enantiomers is outside the temperature range observable.

2.5. Related molecules

For the dimers $[Pt_2H_2(P{-}P_2)_2]$ (Type II, Scheme 1) a fluxional process was observed which renders the four phosphorus nuclei, the hydrides and the platinum centres NMR equivalent. The process that is proposed to explain these observations involves a rotation of one of the PtH(P–P) moieties by 90° around the Pt–Pt bond to give a D_{2h} symmetry for the central moiety [19]. This is followed by hydride exchange between the metal centres with simultaneous twisting of the phosphine ligands by 90° within the principal coordination plane (Scheme 3). A ^{13}CO enriched sample of the dimer $[Pt_2Cp^*_2(CO)_2]$ shows, in the ^{13}C NMR spectrum, a 1:8:18:8:1 multiplet for the carbonyl group. The inner satellites collapse upon lowering the temperature, which is the expected behaviour for the exchange of the terminal CO groups between the platinum atoms.

Further evidence for an intramolecular exchange mechanism comes from the structural data of some closely related platinum(I) dimers which could serve as

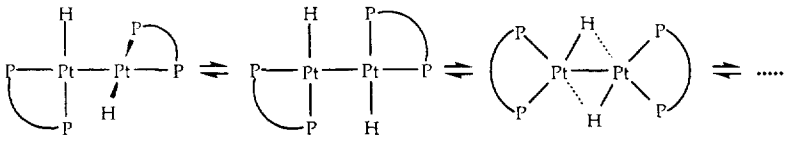

Scheme 3. The mechanism proposed [55] to explain the fluxional process observed in the dimers $[Pt_2H_2(P{-}P)_2]$.

Table 4
Relative total energy, overlap population and atom charge for $[Pt_2Cl_2(CO)_2(PH_3)_2]$ during the mechanism proposed

	Unbridged carbonyl structure	Transition state	Bridged carbonyl structure
Relative total energy ($kJ\,mol^{-1}$)	≡ 0	+ 44	+ 10
Overlap population			
Pt–Pt	0.344	0.146	0.086
Pt–C(1)	0.881	0.750	0.490
Pt–C(2)	0.024	0.169	0.490
Pt–Cl	0.463	0.447	0.421
Pt–P	0.506	0.514	0.545
Atom charge			
Pt	−0.040	0.009	0.091
C	0.713	0.684	0.659
Cl	−0.531	−0.524	−0.511
P	0.208	0.225	0.206

ligands towards the other platinum centre is accompanied by a movement of the phosphine and the chloro ligands to pass a transition state (Step 2), resulting in an intermediate of C_{2h} symmetry (Step 3). Both of the two CO ligands take a bridging position between the platinum centres, giving a planar geometry for the platinum atoms and the principal coordinating atoms.

To rationalise this mechanism, EH molecular orbital calculations were performed on the model compound $[Pt_2Cl_2(CO)_2(PH_3)_2]$. The intermediate represents a local energy minimum with C_{2h} symmetry which is calculated to be only $10\,kJ\,mol^{-1}$ higher than the ground state (Step 1). The barrier for this process is calculated as $44\,kJ\,mol^{-1}$ (Table 4). The corresponding Walsh diagram (Fig. 7) shows an allowed crossing between molecular orbital (MO) 1b, which accounts for the π^*_{Pt-Pt} interaction, and MO 3b, liable for the σ^*_{Pt-Pt} interaction. The following electronic structure of the ground state molecule, $(\pi_{Pt-Pt})^2(\pi^*_{Pt-Pt})^2(\sigma_{Pt-Pt})^2(\sigma^*_{Pt-Pt})^0$, becomes $(\sigma_{Pt-Pt})^2(\sigma^*_{Pt-Pt})^2(\pi^*_{Pt-Pt})^0$ in the intermediate.

The HOMO is strongly stabilised in the intermediate by retrodonation from the $Pt(d_{xy} - d_{xy})$ into the π^* of the CO ligands (MO 1a). This is confirmed by the increase of the positive charge on the platinum atoms and a decrease of the charge on the carbon atoms along the reaction coordinate (Table 4). The overlap population between the platinum atoms decreases sharply, indicating that the Pt–Pt bond is effectively broken. This is compensated by stronger Pt–C bonds, indicated by an increased total overlap population between Pt and C.

The π acceptor ability of the carbonyl ligand is the dominant stabilising factor for the intermediate, and is

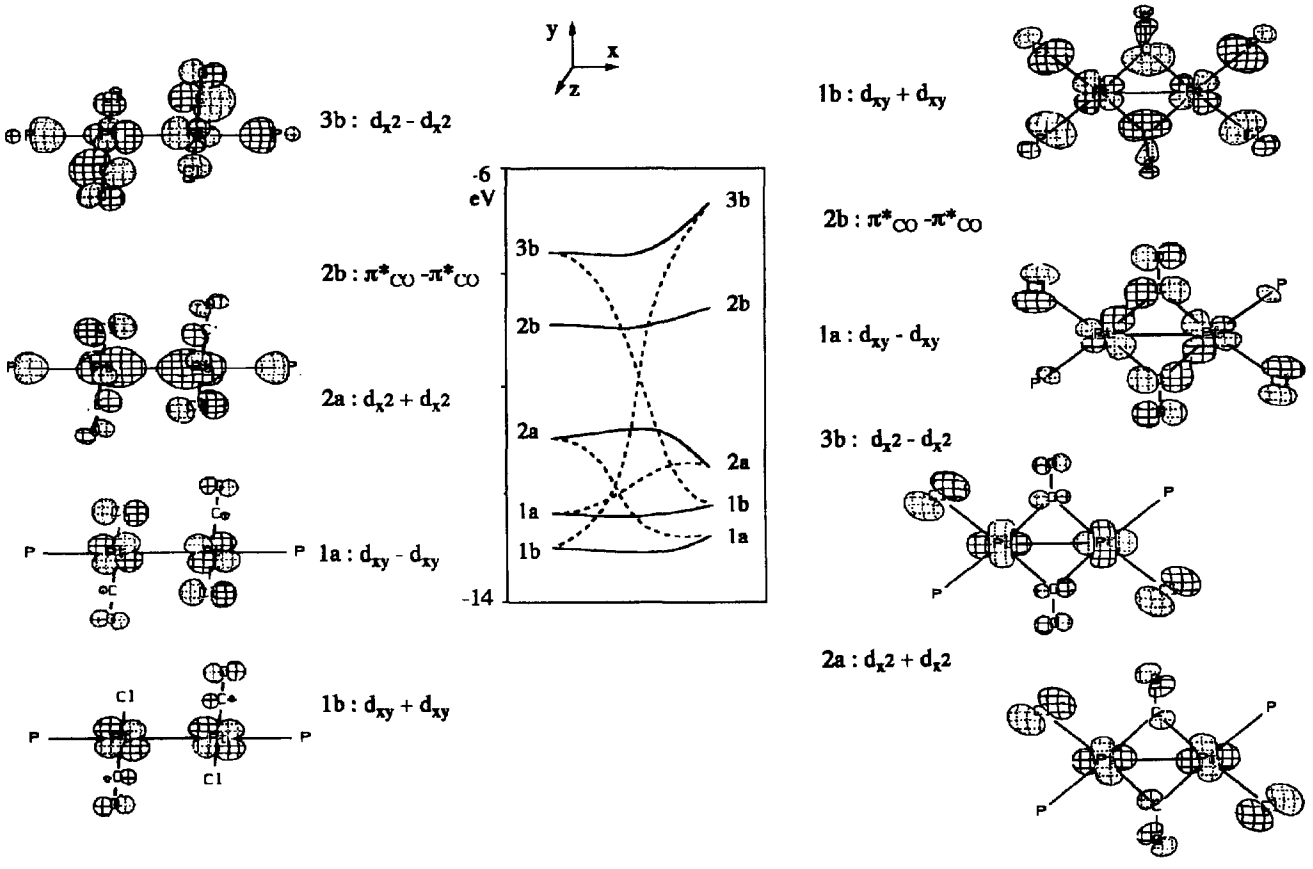

Fig. 7. Walsh diagram for the formation of the carbonyl-bridged intermediate for the model compound $[Pt_2Cl_2(CO)_2(PH_3)_2]$.

essential to explain the energetic aspects of the system. Bridging π donor ligands, e.g. Cl, lead to higher energies, and 263 kJ mol^{-1} was calculated for $[Pt_2(\mu\text{-}Cl)_2(CO)_2(PH_3)_2]$ and 321 kJ mol^{-1} for the transition state. Similar observations were made in theoretical calculations on related dinuclear palladium [43] and platinum [44] compounds. The low energy barrier calculated for this mechanism confirms that a simultaneous migration of the two CO ligands might constitute an explanation for the fluxional process observed in **1a**.

In an attempt to understand the reasons why platinum(I) dimers with bridging ligands and dimers with ligands only in terminal positions are observed, and to further understand the fluxional process, EH calculations have been carried out on two related systems. $[Pt_2H(CO)(PH_3)_4]^+$ and $[Pt_2H_2(PH)_3)_4]$ were used as model systems for the structurally characterised dimers $[Pt_2(\mu\text{-}H)(\mu\text{-}CO)(P\text{–}P)_2]^+$ (compounds **r** and **s**) and $[Pt_2H_2(P\text{–}P)_2]$ (Type II, Scheme 1). The former dimer has two bridging ligands (H and CO), while in the latter compound the two hydride ligands take terminal positions. The calculated ground state of these systems is consistent with the structure observed in the solid state and reproduces the bridging position of the ligands in $[Pt_2H(CO)(PR_3)_4]^+$. The calculated reaction barriers follow the same trends as the coalescence temperatures observed for these dimers in variable temperature experiments, and decrease from $[Pt_2H_2(PH_3)_4]$, $[Pt_2H(CO)(PH_3)_4]^+$ to $[Pt_2Cl_2(CO)_2(PH_3)_2]$ (Table 5).

The MOs, which determine whether bridging or terminal ligands are observed in the solid state, are the HOMO and internal MOs located on the hydride or carbonyl ligands. In $[Pt_2H_2(PH_3)_4]$, the HOMO is the σ_{Pt-Pt} bond in the unbridged structure, which becomes π_{Pt-Pt} antibonding in the bridged structure, as observed in the $[Pt_2Cl_2(CO)_2(PH_3)_2]$ system. The antibonding interaction destabilises the bridged structure and explains the lower energy (64 kJ mol^{-1}) for the unbridged structure. A corresponding antibonding π^*_{Pt-Pt} (MO 1a) interaction occurs in $[Pt_2Cl_2(\mu\text{-}CO)_2(PH_3)_2]$, but the orbital is stabilised considerably by overlap with the π^*_{CO} orbitals. The Pt–H bond is weakest in the transition state, corresponding to a maximal destabilisation of the $1s_H + 1s_H$ combination, and the lowest overlap population between platinum and the two hydride ligands.

In $[Pt_2H(CO)(PH_3)_4]^+$ the bridged structure is found to be more stable (20 kJ mol^{-1}) than the structure with all ligands terminal. The energy of the HOMO is the same in both molecules. The MO, which commands the stability of the system, is localised on the H and CO. The $(1s_H\text{–}2sp_C)$ MO of the H and CO fragment is much more destabilised in the bridged structure than in the unbridged one, consequently the overlap between Pt and H/CO is higher in the bridged structure than in the unbridged one, increasing the stability of the bridged structure. The transition state is calculated to be 61 kJ mol^{-1}, higher than the bridged ground state structure, and a similar allowed crossing as described in $[Pt_2Cl_2(CO)_2(PH_3)_2]$ occurs.

The model compounds $[Pt_2(CO)_2(PH_3)_4]^{2+}$ and $[Pt_2Cl_2(CO)_2(PH_3)_2]$ are found to be very close concerning thermodynamic and electronic aspects. In $[Pt_2(CO)_2(PH_3)_4]^{2+}$, only 1 kJ mol^{-1} energy difference is found between the bridged and the unbridged carbonyl structure. The energy barrier is calculated as 51 kJ mol^{-1}.

The mechanism proposed would also be consistent with the variable temperature NMR data on $[Pt_2Cl_2(^{13}CO)_2(PNpPh_2)_2]$. When the temperature is raised the exchange between the two enantiomers will be faster. On average, a higher proportion of the molecules will pass through the C_{2h} intermediate state and a higher contribution of the intermediate to the average NMR signal is expected. Bridging carbonyls are known to have a more positive chemical shift (more downfield) and a lower coupling constant $^1J(^{13}C,^{195}Pt)$ than terminal carbonyl groups [45]. The coupling constant between directly bonded atoms arises mainly from the Fermi contact interaction between nuclear moments and the electron spins in the bonding orbitals [46]. It can therefore be related to the overlap population calculated in the extended Hückel calculations. The overlap population in the intermediate is lower for the Pt–C bond, but higher for the Pt–P bond relative to the ground state molecule. A lower $^1J(^{13}C,^{195}Pt)$ at higher temperatures

Table 5
Comparison of the calculated energy barriers for intramolecular ligand exchange between the platinum centres with the limiting temperatures measured in variable temperature NMR spectroscopic experiments

	Calculated barrier (kJ mol^{-1})	Limiting temperature (°C)	Observed for L =	Reference
$[Pt_2H_2L_2]$	100 for L = $2PH_3$	−36	$Cy_2P(CH_2)_2PCy_2$	
		−54	$^iPr_2P(CH_2)_2P^iPr_2$	[19]
		< −90	$^tBu_2P(CH_2)_2P^tBu_2$	
$[Pt_2H(CO)L_2]^+$	61 for L = $2PH_3$	−70	$Fe(\eta^5\text{-}C_5H_4PPh_2)_2$	[41]
		−60	$Ph_2P(CH_2)_2PPh_2$	[42]
$[Pt_2Cl_2(CO)_2L_2]$	44 for L = PH_3	−110	$PNpPh_2$	this work

is therefore consistent with this mechanism. The larger changes observed in the two bond coupling constants are connected with more variables, and cannot be explained without further calculations.

2.7. Conclusions

The unbridged platinum(I) dimers $[Pt_2Cl_2(CO)_2(PR_3)_2]$ ($PR_3 = PNpPh_2$ and PFc_2Ph) have been synthesised by reduction of $[PtCl_2(COD)]$ in the presence of CO and the appropriate polyaromatic phosphine. Slight variations of the reaction conditions lead to the isolation of the platinum *triangulo-* cluster compounds $[Pt_3(\mu\text{-}CO)_3(PR_3)_3]$ ($PR_3 = PNpPh_2$ and PNp_2Ph). The structure of the dimer $[Pt_2Cl_2(CO)_2(PFc_2Ph)_2] \cdot 3CHCl_3$ was determined by a single crystal X-ray diffraction study. The complex was shown to consist of two square-planar PtCl(CO)(PFc_2Ph) units bonded via a direct metal–metal bond. The two principal coordination planes are approximately perpendicular to each other, rendering the molecule chiral. $^{31}P\{^1H\}$ NMR studies have indicated a fluxional process which renders the two halves of this type of platinum dimer equivalent on the NMR timescale. A mechanism for this process is suggested on the basis of NMR and structural data and was explored using theoretical calculations. The mechanism consists of a concerted motion of all ligands, resulting effectively in an exchange of CO between the platinum centres.

3. Experimental

3.1. General

Standard Schlenk techniques and a nitrogen atmosphere were used routinely for carrying out the reactions, but no special precautions were taken to exclude oxygen during work-up procedures, unless otherwise stated. Solvents were of reagent grade and used as purchased for chromatography. For all synthetic reactions the solvents were dried by published methods [47] and distilled under N_2. ^{13}CO was prepared by reaction of ^{13}C-formic acid with degassed H_2SO_4(conc) at 60 °C and purified by passing over KOH pellets. The phosphines were prepared following modified literature [48] methods, carefully excluding oxygen during all steps to minimise the oxidation to the corresponding phosphine oxides. Diferrocenylphenylphosphine was purchased from Aldrich. Infrared spectra were recorded on a Perkin–Elmer 1720 infrared Fourier transform spectrometer as KBr pellets unless otherwise stated. The low frequency limit for the observation of IR signals was 300 cm^{-1}. Raman spectra were obtained on a Perkin–Elmer NIR FT-Raman 1700X spectrometer equipped with an NdYAG-laser (1064 nm). ^1H, $^{31}P\{^1H\}$, $^{13}C\{^1H\}$ and ^{195}Pt NMR spectra were recorded on a JEOL JNM-EX270 Fourier transform NMR spectrometer with chemical shifts reported relative to TMS, H_3PO_4 and Na_2PtCl_6(aq). For the $^{31}P\{^1H\}$ spectra $PO(OMe)_3$ was used as internal reference using the conversion $\delta(PO(OMe)_3) = \delta(H_3PO_4) + 3.0$ ppm. Mass spectra were recorded on a VG AutoSpec-Q as FAB using 3-NBA as matrix.

3.2. Preparation of $[PtCl_2(COD)]$

Platinum metal (1.40 g, 7.18 mmol) was dissolved in aqua regia (50 cm^3) at 60 °C by stirring the mixture overnight. The excess nitrogen oxides were removed by reducing the volume of the solution on an open hotplate while keeping the volume constant by adding HCl_{aq}(conc). After all the brown colour had disappeared the solution was carefully reduced to dryness. The residue was then dissolved in a mixture of distilled water (20 cm^3) and n-propanol (15 cm^3). Cyclooctadiene (3 cm^3, 24.5 mmol) and $SnCl_2 \cdot 2H_2O$ (1.645 g, 7.287 mmol, 1.5% excess) were added and the mixture stirred until the brown colour had disappeared (seven days, RT 12 °C). The white precipitate was filtered off, washed with distilled water (20 cm^3) and EtOH (3 cm^3) and dried over silica gel.

Yield 2.54 g, 95%. Anal. Found: C, 25.5; H, 3.1. $C_8H_{12}Cl_2Pt$ Calc.: C, 25.7; H, 3.2%. ^1H NMR ($CDCl_3$): δ 5.62 (t, $^2J(^1H,^{195}Pt)$ 66.2, $^3J(^1H,^1H)$ 3.0 Hz, 4H), 2.74 (m, $^2J(^1H,^1H)$ 9.0, $^3J(^1H,^1H)$ 3.0 Hz, 4H), 2.3 (m, $^2J(^1H,^1H)$ 9.0 Hz, 4H). $^{13}C\{^1H\}$ NMR ($CDCl_3$): δ 100.1 (t, $^1J(^{13}C,^{195}Pt)$ 153 Hz), 30.9 (s). $^{195}Pt\{^1H\}$ NMR ($CDCl_3$): δ −3337.3 (s). $\tilde{\nu}_{max}/cm^{-1}$ 3008s, 1476s, 1340vs, 1010s, 832s, 475s, 338s ν(Pt–Cl), 319vs ν(Pt–Cl).

3.3. Preparation of $[Pt_2Cl_2(CO)_2(PNpPh_2)_2]$ (1a)

$[PtCl_2(COD)]$ (0.187 g, 0.5 mmol) and $PNpPh_2$ (0.156 g, 0.5 mmol) were dissolved in $CHCl_3$ (40 cm^3) and the solution saturated with CO (excess) or ^{13}CO (generated from 0.25 g, 5.3 mmol $H^{13}COOH$) for 30 min. The solution was cooled to −50 °C, a solution of $LiEt_3BH$ in THF (1 M, 0.5 cm^3) added, and slowly warmed to ambient temperatures. After stirring overnight the mixture was filtered, heptane added, and the volume reduced until all $CHCl_3$ was removed. The precipitate was filtered off and dried in vacuo (0.190 g, 45% **1a**). The crude product was dissolved in a minimum of $CHCl_3$ (ca. 10 cm^3) and transferred to the top of a chromatography column (dimensions 24 × 3.5 cm^2, silica gel 70–230 mesh). The column was eluted with CH_2Cl_2, giving first a yellow band. The eluate was reduced to a small volume, the product precipitated with hexane and dried in vacuo.

Yield 0.088 g, 29%. Anal. Found: C, 49.3; H, 3.3. $C_{46}H_{34}Cl_2O_2P_2Pt_2$ Calc.: C, 48.4; H, 3.0%. ^{1}H NMR ($CDCl_3$): δ 8.5–7.1 (m). $^{13}C\{^1H\}$ NMR ($CDCl_3$): δ 168.8 (s, CO), 136.1–124.7 (m). $^{31}P\{^1H\}$ NMR ($CDCl_3$): δ 30.0 (m, $^1J(^{31}P,^{195}Pt)$ 2189, $^2J(^{31}P,^{195}Pt)$ 470, $^3J(^{31}P,^{31}P)$ 233 Hz). $^{195}Pt\{^1H\}$ NMR ($CDCl_3$): δ −3940 (dd, $^1J(^{195}Pt,^{31}P)$ 2189, $^2J(^{195}Pt,^{31}P)$ 463 Hz). $\tilde{\nu}_{max}/cm^{-1}$ 2052vs, 2036vs ν_{sym}(CO), 322m ν(PtCl), bands characteristic for $PNpPh_2$. Raman: 193m ν(PtPt). *m/z* 1141 (M^+), 1105 ($M - Cl^-$), 1078 ($M - Cl^- - CO$), 1049 $M - Cl^- - 2CO$). Accurate mass spectrum: *m/z* 1105.103; $C_{46}H_{34}ClO_2P_2{}^{195}Pt_2$ Calc.: 1105.102, 1078.106; $C_{45}H_{34}ClOP_2{}^{195}Pt{}^{196}Pt$ Calc.: 1078.107, 1049.101; $C_{44}H_{33}ClP_2{}^{195}Pt{}^{196}Pt$ Calc.: 1049.104.

Different for $[Pt_2Cl_2(^{13}CO)_2(PNpPh_2)_2]$. $^{13}C\{^1H\}$ NMR ($CDCl_3$): δ 168.8 (t, $^1J(^{13}C,^{195}Pt)$ 1958 Hz, CO), 136.7–125.4 (m). $^{195}Pt\{^1H\}$ NMR ($CDCl_3$): δ −3940 (dddd, $^1J(^{195}Pt,^{31}P)$ 2197, $^2J(^{195}Pt,^{31}P)$ 474, $^1J(^{195}Pt,^{13}C)$ 1958, $^2J(^{195}Pt,^{13}C)$ 32 Hz). $\tilde{\nu}_{max}/cm^{-1}$ (KBr) 2002vs, 1987vs ν(CO), 322m ν(PtCl). $\tilde{\nu}_{max}/cm^{-1}$ ($CHCl_3$) 2009vs, 1992vs ν(CO).

3.4. Preparation of $[Pt_2Cl_2(CO)_2(PFc_2Ph)_2] \cdot 3CHCl_3$ (1b)

$[PtCl_2(COD)]$ (0.187 g, 0.5 mmol) and PFc_2Ph (0.239 g, 0.5 mmol) were dissolved in $CHCl_3$ (40 cm^3) and CO bubbled through the solution for 30 min. The solution was cooled to −60 °C and a solution of $LiBHEt_3$ in THF (1 M, 0.5 cm^3) added. The solution was kept in the freezer at −25 °C for two months, during which time the reaction was followed by $^{31}P\{^1H\}$ NMR spectroscopy. When the maximum concentration of the dimer ($\delta(^{31}P) = 26.6$, 29%) was obtained, the mixture was filtered, warmed to ambient temperatures and the products separated using thin layer chromatography (silica gel, eluent 4:1 $CHCl_3$–hexane). The second, yellow band was scratched from the glass plate, the material extracted with CH_2Cl_2 and the solvent removed in vacuo. Crystals suitable for the X-ray crystal structure determination were grown by slow evaporation of a chloroform solution over two weeks at 4 °C.

Yield 0.035 g, 9.5%. Anal. Found: C, 37.5; H, 2.5. Three $CHCl_3$ solvent molecules, $C_{57}H_{49}Cl_8Fe_4O_2P_2Pt_2$ Calc.: C, 37.4; H, 2.7%. ^{1}H NMR ($CDCl_3$): δ 7.6 (m, 2H), 7.4 (m, 3H), 4.4–4.2 (m, 18H). $^{31}P\{^1H\}$ NMR ($CDCl_3$): δ 26.5 (m, $^1J(^{31}P,^{195}Pt)$ 2437, $^2J(^{31}P,^{195}Pt)$ 413, $^3J(^{31}P,^{31}P)$ 239 Hz). $^{13}C\{^1H\}$ NMR ($CDCl_3$): δ 170.5 (s), 134.1 (m), 130.4 (s), 127.7 (m), 74.3–69.5 (m). $^{195}Pt\{^1H\}$ NMR ($CDCl_3$): δ −3969 (dd, $^1J(^{195}Pt,^{31}P)$ 2436, $^2J(^{195}Pt,^{31}P)$ 416 Hz). $\tilde{\nu}_{max}/cm^{-1}$ 2032vs, 2018vs ν_{sym}(CO), 324m ν(PtCl), bands characteristic for PFc_2Ph. Raman: 190m ν(PtPt). *m/z* 1472 (M^+), 1444 ($M^+ - CO$), 1436 ($M^+ - Cl$). Accurate mass spectrum: *m/z* 1471.929; $C_{54}H_{46}O_2Cl_2{}^{56}Fe_4P_2{}^{195}Pt_2$ Calc.: 1471.904.

The precipitate filtered from the reaction mixture was recrystallised from CH_2Cl_2/hexane and identified as $[PtClH(PFc_2Ph)_2]$.

Yield 0.046 g, 8%. Anal. Found: C, 50.8; H, 3.9. One CH_2Cl_2 solvent molecule, $C_{53}H_{49}Cl_3Fe_4P_2Pt$ Calc.: C, 50.0; H, 3.9%. ^{1}H NMR ($CDCl_3$): δ 8.0 (m, 4H), 7.4 (m, 6H), 4.6–4.3 (m, 36H), −16.7 (tt, $^1J(^1H,^{195}Pt)$ 610, $^2J(^1H,^{31}P)$ 16 Hz). $^{31}P\{^1H\}$ NMR ($CDCl_3$): δ 9.2 (t, $^1J(^{31}P,^{195}Pt)$ 3073 Hz). $\tilde{\nu}_{max}/cm^{-1}$ 2183m ν(PtH), 327w ν(PtCl).

3.4.1. Crystal structure determination of (1b)

Crystal data for (1b). $C_{56}H_{48}Cl_8Fe_4O_2P_2Pt_2$, M = 1712.06, monoclinic, a = 18.826(5), b = 13.0717(8), c = 50.192(3) Å, β = 99.426(13)°, U = 12185(3) Å^3, space group $C2/c$, Z = 8, D_c = 1.867 Mg m^{-3}, $F(000)$ = 6608, orange block, crystal dimensions 0.23 × 0.20 × 0.17 mm^3, the crystal was coated in araldite to prevent rapid desolvation, μ(Cu Kα) = 198.39 cm^{-1}.

Data collection and processing. Siemens P4/PC rotating anode diffractometer, ω scans using graphite monochromated Cu Kα radiation. Attempts to collect data using Mo radiation failed because of insufficient peak separation due to the 50 Å c-axis. 9258 reflections were collected, of which 5952 were unique and observed ($2\theta \leq 120°$, $I > 2\sigma(I)$).

Structure analysis and refinement. The structure was solved by direct methods [49]. Full-matrix anisotropic refinement of all non-hydrogen atoms based on F^2 produced R_1 = 0.0656 and wR_2 = 0.1769 using absorption corrected data (SHELXA-90); max. and min. transmission factors were 0.3093 and 0.0355. Two of the co-crystallised chloroform molecules are disordered. One is disordered around a special position; the second is disordered forming a half-occupied pseudo-tetrahedron. A proton for this chloroform was not located. The remaining protons were positioned based on the geometry of their parent atoms using standard bond lengths. Atom coordinates are listed in Table 6. Further details of the crystal study are available from the director of the Cambridge Crystallographic Data Centre, 12 Union Road, Cambridge CB2 1EZ, UK.

3.5. Preparation of $[Pt_2Cl_2(CO)_2(PAn_2Ph)_2]$ (1c)

The compound was prepared in the same way as $[Pt_2Cl_2(CO)_2(PFc_2Ph)_2]$. The maximum concentration of the dimer ($\delta(^{31}P) = 10.3$) in the reaction mixture was ca. 37%. The dimer decomposed when the solution was warmed to room temperature.

$^{31}P\{^1H\}$ NMR ($CDCl_3$): δ 10.3 (m, $^1J(^{31}P,^{195}Pt)$ 2044, $^2J(^{31}P,^{195}Pt)$ 547, $^3J(^{31}P,^{31}P)$ 246 Hz).

3.6. Preparation of $[Pt_3(CO)_3(PNpPh_2)_3]$ (3a)

$[PtCl_2(COD)]$ (0.400 g, 1.07 mmol) was dissolved in $CHCl_3$ (40 cm^3) and CO bubbled through the solution

Table 6
Atomic coordinates ($\times 10^4$) and equivalent isotropic displacement coefficients ($Å^2 \times 10^4$) for $[Pt_2Cl_2(CO)_2(PFc_2Ph)_2]\cdot CHCl_3$ (**1b**)

Pt(1)	1332(1)	348(1)	1450(1)	60(1)
P(2)	583(2)	483(2)	1774(1)	55(1)
C(3)	−121(7)	−497(10)	1732(3)	62(3)
C(4)	−407(8)	−1017(12)	1939(3)	79(4)
C(5)	−988(9)	−1604(14)	1817(4)	102(6)
C(6)	−1042(9)	−1456(12)	1536(4)	94(5)
C(7)	−519(7)	−764(10)	1474(3)	69(4)
Fe(8)	−63(1)	−2018(2)	1679(1)	77(1)
C(9)	603(15)	−2681(17)	1453(6)	128(8)
C(10)	−11(16)	−3299(18)	1456(7)	147(10)
C(11)	3(14)	−3568(15)	1720(6)	129(8)
C(12)	599(12)	−3106(15)	1881(5)	122(8)
C(13)	958(11)	−2559(13)	1724(6)	117(7)
C(14)	976(7)	359(10)	2119(3)	61(3)
C(15)	807(9)	975(11)	2336(3)	74(4)
C(16)	1171(10)	604(15)	2583(3)	95(5)
C(17)	1595(10)	−226(13)	2529(3)	89(5)
C(18)	1469(9)	−372(11)	2238(3)	75(4)
Fe(19)	1872(1)	1054(2)	2333(1)	83(1)
C(20)	2917(15)	1358(33)	2499(5)	172(15)
C(21)	2874(12)	1188(23)	2219(6)	140(9)
C(22)	2399(12)	1914(20)	2076(4)	116(7)
C(23)	2145(13)	2558(17)	2258(5)	126(8)
C(24)	2433(19)	2279(27)	2519(7)	173(14)
C(25)	90(8)	1655(10)	1758(3)	62(3)
C(26)	434(9)	2606(10)	1749(3)	80(4)
C(27)	51(11)	3511(12)	1730(4)	94(5)
C(28)	−690(11)	3511(13)	1722(4)	95(5)
C(29)	−1039(9)	2588(13)	1742(3)	87(5)
C(30)	−669(8)	1664(11)	1751(3)	72(4)
C(31)	2041(9)	−469(12)	1638(3)	77(4)
O(32)	2491(7)	−941(11)	1741(3)	120(5)
Cl(33)	537(3)	1328(4)	1157(1)	110(2)
Pt(41)	2182(1)	368(1)	1084(1)	60(1)
P(42)	2866(2)	678(2)	742(1)	57(1)
C(43)	3659(7)	−129(10)	761(3)	62(3)
C(44)	4083(8)	−482(9)	994(3)	71(4)
C(45)	4663(10)	−1005(14)	944(5)	105(6)
C(46)	4583(10)	−1015(14)	649(5)	111(7)
C(47)	3941(9)	−487(12)	538(4)	92(5)
Fe(48)	3705(1)	−1670(2)	771(1)	80(1)
C(49)	3662(15)	−3023(16)	976(5)	125(8)
C(50)	3046(13)	−2490(16)	994(6)	125(8)
C(51)	2703(12)	−2294(13)	736(5)	110(7)
C(52)	3078(15)	−2701(20)	553(6)	141(9)
C(53)	3744(14)	−3181(13)	712(7)	138(10)
C(54)	2417(7)	565(10)	400(3)	63(3)
C(55)	2540(9)	1218(12)	182(3)	77(4)
C(56)	2128(11)	846(17)	−61(3)	103(6)
C(57)	1761(10)	−39(15)	1(3)	92(5)
C(58)	1932(9)	−205(12)	288(3)	78(4)
Fe(59)	1470(1)	1183(2)	211(1)	75(1)
C(60)	405(10)	1467(17)	65(4)	105(6)
C(61)	511(11)	1180(17)	341(5)	120(7)
C(62)	1165(10)	2602(14)	310(4)	99(5)
C(62)	971(12)	1906(17)	498(4)	110(6)
C(64)	823(10)	2313(17)	42(4)	109(6)
C(65)	3230(6)	1973(5)	756(2)	72(4)
C(66)	2800(5)	2789(7)	809(2)	85(5)
C(67)	3072(7)	3780(6)	819(2)	108(7)
C(68)	3773(8)	3955(6)	777(2)	120(8)
C(69)	4203(6)	3139(9)	724(2)	97(6)
C(70)	3932(5)	2148(8)	714(2)	83(4)
C(71)	1444(8)	−348(14)	895(3)	79(4)
O(72)	983(7)	−836(11)	793(2)	112(4)
Cl(73)	3041(2)	1203(4)	1390(1)	93(1)
C(75)	1867(16)	5020(16)	1500(4)	172(11)
Cl(76)	2390(6)	5773(6)	1331(2)	205(4)
Cl(77)	2143(6)	5011(8)	1828(2)	220(4)
Cl(78)	1733(5)	3834(6)	1364(2)	191(3)
C(80)	19(23)	4483(24)	2381(9)	[a]160(21)
Cl(81)	0	5668(11)	2500	[a]300(10)
Cl(82)	726(9)	3820(10)	2541(3)	331(8)
C(85)	956(26)	−3928(26)	366(7)	[a]379(64)
Cl(86)	863(10)	−3619(20)	677(5)	[b]249(16)
Cl(87)	1052(10)	−2836(10)	202(5)	[b]240(15)
Cl(88)	1683(11)	−4636(11)	353(5)	[b]202(11)
Cl(89)	425(17)	−4724(16)	128(5)	[b]206(12)

[a] Site occupancy 0.5. [b] Site occupancy 0.38.

for 1 h. A solution of $PNpPh_2$ (0.334 g, 1.07 mmol) in $CHCl_3$ (30 cm^3) was added. The mixture was stirred for 5 min, heptane added and the volume reduced to dryness. Most of the residue was dissolved in a minimum amount of CH_2Cl_2, the solution was filtered, the filtrate run into a large amount of hexane (250 cm^3) which had been saturated with CO and the mixture stirred for 30 min. The precipitate of $[PtCl_2(CO)(PNpPh_2)]$ (**2a**) was filtered off and dried in vacuo. The product was still impure at this stage, as shown by ^1H and ^{31}P NMR spectroscopy, but was used without further purification.

Yield 0.519 g, 80%. Anal. Found: C, 45.7; H, 2.9. $C_{23}H_{17}Cl_2OPPt$ Calc.: C, 45.5; H, 2.8%. ^1H NMR ($CDCl_3$): δ 8.2–7.1 (m). $^{31}P\{^1H\}$ NMR ($CDCl_3$): δ 5.7 (t, $^1J(^{31}P,^{195}Pt)$ 3057 Hz). ^{195}Pt NMR ($CDCl_3$): δ −4042 (d, $^1J(^{195}Pt,^{31}P)$ 3062 Hz). $\tilde{\nu}_{max}/cm^{-1}$ 2104vs $\nu_{sym}(CO)$. m/z 882 ($M - Cl^- + PNpPh_2$).

The crude $[PtCl_2(CO)(PNpPh_2)]$ (0.400 g) was dissolved in THF. The solution was saturated with CO (20 min), zinc powder (100 mesh, ca. five-fold excess) was added and the mixture stirred until the initially developing green colour turned to red (24 h). The solution was filtered off, hexane added and the volume reduced in vacuo. The precipitate was filtered off and dried in air (0.384 g). The crude product (0.100 g) was dissolved in a minimum of CH_2Cl_2 (ca. 5 cm^3) and transferred to the top of a chromatography column (dimensions 18 × 2.5 cm^2, silica gel 70–230 mesh). The column was eluted with CH_2Cl_2, giving an orange band. The eluate of this band was reduced to 5 cm^3, the product precipitated with hexane and dried in vacuo (0.054 g).

Overall yield, based on $[Pt(COD)Cl_2]$, 59%. Anal. Found: C, 49.8; H, 2.9. One CH_2Cl_2 solvent molecule, $C_{70}H_{53}Cl_2O_3P_3Pt_3$ Calc.: C, 49.7; H, 3.1%. ^1H NMR ($CDCl_3$): δ 8.3 (d), 7.9 (d), 7.5–7.1 (m). $^{13}C\{^1H\}$ NMR ($CDCl_3$): δ 243.2 (s), 135.2–124.7 (m). $^{31}P\{^1H\}$ NMR

($CDCl_3$): δ 50.6 (m, $^1J(^{31}P,^{195}Pt)$ 4917, $^2J(^{31}P,^{195}Pt)$ 482, $^3J(^{31}P,^{31}P)$ 54 Hz). $^{195}Pt\{^1H\}$ NMR ($CDCl_3$): δ −4536 (dd, $^1J(^{195}Pt,^{31}P)$ 4925, $^2J(^{195}Pt,^{31}P)$ 479 Hz). $\tilde{\nu}_{max}/cm^{-1}$ 1795vs $\nu_{sym}(CO)$, bands characteristic for $PNpPh_2$. *m/z* 1550 ($M^+ - 2CO$).

3.7. Preparation of $[Pt_3(CO)_3(PNp_2Ph)_3]$ (3b)

$[PtCl_2(COD)]$ (0.400 g, 1.07 mmol) was dissolved in $CHCl_3$ (40 cm^3) and CO bubbled through the solution for 1 h. A solution of PNp_2Ph (0.387 g, 1.07 mmol) in CH_2Cl_2 (30 cm^3) was added. The mixture was stirred for 5 min, heptane added and the volume reduced to dryness. The residue was dissolved in a minimum amount of CH_2Cl_2, the solution filtered, the filtrate run into a large amount of hexane (250 cm^3) which had been saturated with CO and the mixture stirred for 1 h. The precipitate of $[PtCl_2(CO)(PNp_2Ph)]$ (**2b**) was filtered off and dried in vacuo. The product was still impure at this stage, as shown by ^1H and ^{31}P NMR spectroscopy, but was used without further purification.

Yield 0.295 g, 52%. ^1H NMR ($CDCl_3$): δ 8.3–7.0 (m). $^{31}P\{^1H\}$ NMR ($CDCl_3$): δ 3.2 (t, $^1J(^{31}P,^{195}Pt)$ 3021 Hz). $\tilde{\nu}_{max}/cm^{-1}$ 2101 vs $\nu_{sym}(CO)$. *m/z* 983 ($M - Cl^- + PNpPh_2$).

The crude $[PtCl_2(CO)(PNp_2Ph)]$ (0.400 g) was dissolved in THF. The solution was saturated with CO (20 min), zinc powder (100 mesh, ca. five-fold excess) was added and the mixture stirred until the initially developing green colour turned to dark red (24 h). The solution was filtered off, heptane added and the solvent partially removed in vacuo. The precipitate was filtered off and dried in air (0.213 g). The crude product (0.100 g) was dissolved in a minimum of CH_2Cl_2 (ca. 5 cm^3) and transferred to the top of a chromatography column (dimensions 18 × 2.5 cm^2, silica gel 70–230 mesh). The column was eluted with CH_2Cl_2, giving an orange band. The eluate of this band was reduced to 5 cm^3, the product precipitated with hexane and dried in vacuo (0.029 g).

Overall yield, based on $[PtCl_2(COD)]$, 18%. Anal. Found: C, 53.9, H, 3.2. $C_{81}H_{57}O_3P_3Pt_3$ Calc.: C, 55.4; H, 3.2%. ^1H NMR ($CDCl_3/CD_2Cl_2$): δ 8.3–6.7 (m). $^{31}P\{^1H\}$ NMR ($CDCl_3/CD_2Cl_2$): δ 48.3 (m, $^1J(^{31}P,^{195}Pt)$ 4786, $^2J(^{31}P,^{195}Pt)$ 497, $^3J(^{31}P,^{31}P)$ 57 Hz). $\tilde{\nu}_{max}/cm^{-1}$ 1793vs $\nu_{sym}(CO)$, bands characteristic for PNp_2Ph.

3.8. EH calculations

EHMO calculations [50–52] were carried out on idealised model systems. The interatomic distances were based on X-ray crystal structures [9,14,41,42], compound **1b** with Pt–Pt = 2.62, Pt–P = 2.37, Pt–Cl = 2.30, Pt–H = 1.55, Pt–C = 1.80, *C–O* = 1.10 Å. The geometry of PH_3 was set as experimentally observed [53]. All calculation parameters were taken from the literature [54]. For $[Pt_2Cl_2(CO)_2(PH_3)_2]$, $[Pt_2(CO)_2(PH_3)_4]^{2+}$ and $[Pt_2(H)_2(PH_3)_4]$ the calculations were performed with respect to a C_2 axis. For $[Pt_2(H)(CO)(PH_3)_4]^+$ no element of symmetry was used.

Six steps were calculated for each model compound. The following parameters with their limiting values were used as variables [36,37]: $[Pt_2Cl_2(CO)_2(PH_3)_2]$, formation of the carbonyl bridged intermediate, Pt–C = 1.80, 2.04 Å, Pt–Pt–C = 90.0, 49.6°, Pt–C–O = 180.0, 139.6°, Pt–Pt–Cl = 90.0, 135.0°, Pt–Pt–P = 90.0, 135.0°, dihedral angle between the two principal coordination planes ϕ = 45.0, 0.0°; $[Pt_2Cl_2(CO)_2(PH_3)_2]$, formation of the chloride bridged intermediate, Pt–Pt = 2.62, 3.60 Å, Pt–Cl = 2.30, 2.40 Å, Pt–Pt–Cl = 90.0, 40.7°, Pt–Pt–C = 90.0, 135.0°, Pt–Pt–P = 90.0, 135.0°, ϕ = 45.0, 0.0°; $[Pt_2(CO)_2(PH_3)_4]^{2+}$, Pt–C = 1.80, 2.04 Å, Pt–Pt–C = 90.0, 49.6°, Pt–C–O = 180.0, 139.6°, Pt–Pt–P = 90.0, 135.0°, ϕ = 45.0, 0.0°; $[Pt_2H_2(PH_3)_4]$, formation of the hydride bridged intermediate, Pt–H = 1.55, 1.77 Å, Pt–Pt–P = 90.0, 141.8°, 135.0°, ϕ = 45.0, 0.0°; $[Pt_2H(CO)(PH_3)_4]^+$, formation of the intermediate with one bridging hydride and one bridging carbonyl ligand, Pt–Pt = 2.64, 2.72 Å, Pt–C = 1.80, 2.04 Å, Pt–Pt–C = 90.0, 48.2°, Pt–C–O = 180.0, 138.2°, Pt–Pt–H = 90.0, 28.7°, Pt–Pt–P = 90.0, 135.0°, ϕ = 45.0, 0.0°. The Pt–H bond distance was kept constant at 1.55 Å.[56]

Acknowledgements

Acknowledgement BP is thanked for their generous endowment of D.M.P.M.'s chair and SERC for funding for the diffractometers. T. Woodroffe and Professor McPartlin are thanked for the determination of the unit cell dimensions of **1b**.

References

[1] D.M.P. Mingos and T.E. Müller, *J. Organomet. Chem.*, *500* (1995) 251.
[2] T.E. Müller, S.W.K. Choi, D.M.P. Mingos, D. Murphy, D.J. Williams and V.W.W. Yam, *J. Organomet. Chem.*, *484* (1994) 209.
[3] T.E. Müller, D.M.P. Mingos and D.J. Williams, *J. Chem. Soc., Chem. Commun.*, *15* (1994) 1787.
[4] T.E. Müller and D.M.P. Mingos, *Trans. Met. Chem.*, *20* (1995) 533.
[5] T.E. Müller, J.C. Green, S. Menzer, D.M.P. Mingos, M. McPartlin, D.J. Williams, C. Whittingham and T. Woodroffe, *J. Organomet. Chem.*, in press.
[6] T.E. Müller, *Thesis*, Imperial College, 1995.
[7] A.D. Burrows and D.M.P. Mingos, *Coord. Chem. Rev.*, in press.
[8] G.K. Anderson, *Adv. Organomet. Chem.*, *35* (1993) 1.
[9] C. Couture, D.H. Farrar, D.S. Fisher and R.R. Gukathasan, *Organometallics*, *6* (1987) 532.
[10] N.M. Boag, J. Browning, C. Crocker, P.L. Goggin, R.J. Good-

fellow, M. Murray and J.L. Spencer, *J. Chem. Res. (S)*, (1978) 228; *J. Chem. Res. (M)*, (1978) 2962.
[11] P.L. Goggin and R. Goodfellow, *J. Chem. Soc., Dalton Trans.*, (1973) 2355.
[12] J.R. Boehm, D.J. Doonan and A.L. Balch, *J. Am. Chem. Soc., 98* (1976) 4845.
[13] S. Fallis and G.K. Erson, *J. Organomet. Chem., 474* (1994) 223.
[14] Y. Yamamoto, K. Takahashi and H. Yamazaki, *Chem. Lett.*, (1985) 201.
[15] T. Tanase, H. Ukaji, Y. Kudo, M. Ohno, K. Kobayashi and Y. Yamamoto, *Organometallics, 13* (1994) 1374.
[16] N.M. Boag, *Organometallics, 7* (1988) 1446.
[17] C.E. Briant, D.I. Gilmour and D.M.P. Mingos, *J. Organomet. Chem., 308* (1986) 381.
[18] R. Uson, J. Fornies, P. Espinet, C. Fortuno, M. Tomas and A.J. Welch, *J. Chem. Soc., Dalton Trans.*, (1989) 1583.
[19] D.J. Schwartz and R. Andersen, *J. Am. Chem. Soc., 117* (1995) 4014.
[20] P.H.M. Buzelaar, *GeNMR, Vers. 3.4 r2*, Ivorysoft, 1993.
[21] A. Moor, P.S. Pregosin and L.M. Venanzi, *Inorg. Chim. Acta, 48* (1981) 153.
[22] D.M.P. Mingos and R.W.M. Wardle, *Trans. Met. Chem., 10* (1985) 441.
[23] T. Yoshida, T. Yamagata, T.H. Tulip, J.A. Ibers and S. Otsuka, *J. Am. Chem. Soc., 100* (1978) 2062.
[24] *Cambridge Structural Database*, Vers. 508, August 1994; F.H. Allen, J.E. Davies, J.J. Galloy, O. Johnson, O. Kennard, C.F. Macrae, E.M. Mitchell, G.F. Mitchell, J.M. Smith and D.G. Watson, *J. Chem. Inf. Comp. Sci., 31* (1991) 187.
[25] J.J. Novoa, G. Aullon, P. Alemany and S. Alvarez, *J. Am. Chem. Soc., 117* (1995) 7169.
[26] K.W. Browall, T. Bursh, L.V. Interrante and J.S. Kasper, *Inorg. Chem., 11* (1972) 1800.
[27] E. Hoyer, W. Dietzsch, H. Hennig and W. Schroth, *Chem. Ber., 102* (1969) 603.
[28] A. Dedieu and R. Hoffmann, *J. Am. Chem. Soc., 100* (1978) 2074.
[29] W. Kemp, *NMR in Chemistry, A Multinuclear Introduction*, Macmillan Press, London, 1986, p. 165.
[30] M. Kainosho, K. Ajisaka, W.H. Pirkle and S.D. Beare, *J. Am. Chem. Soc., 94* (1972) 5924.
[31] A. Mannschreck, V. Jones and B. Kolb, *Angew. Chem., 13* (1973) 590.
[32] D. Casarini, L. Lunazzi, G. Placucci and D. Macciantelli, *J. Org. Chem., 52* (1987) 4721.
[33] F. Lefèvre, T. Burgemeister and A. Mannschreck, *Tetrahedron Lett., 13* (1977) 1125.
[34] D. Casarini, S. Davalli and L. Lunazzi, *J. Org. Chem., 54* (1989) 4616.
[35] F. Gasparrini, L. Lunazzi, D. Misiti and C. Villani, *Acc. Chem. Res., 28* (1995) 163.
[36] R. Bender, P. Braunstein, A. Tiripicchio and M. Tiripicchio-Camellini, *J. Chem. Soc., Chem. Commun.*, (1984) 42.
[37] R.J. Goodfellow, I.R. Herbert and A.G. Orpen, *J. Chem. Soc., Chem. Commun.*, (1983) 1386.
[38] H. Jun, V.G. Young and R.J. Angelici, *J. Am. Chem. Soc., 113* (1991) 9379.
[39] E. Baralt, E.A. Boudreaux, J.N. Demas, P.G. Lenhert, C.M. Lukehart, A.T. McPhail, D.R. McPhail, J.B. Myers, L.A. Sacksteder and W.R. True, *Organometallics, 8* (1989) 2417.
[40] D. Afzal, P.G. Lenhert and C.M. Lukehart, *J. Am. Chem. Soc., 106* (1984) 3050.
[41] G. Minghetti, A.L. Bandini, G. Banditelli, F. Bonati, R. Szostak, C.E. Strouse, C.B. Knobler and H.D. Kaesz, *Inorg. Chem., 22* (1983) 2332.
[42] A.L. Bandini, G. Banditelli, M.A. Cinellu, G. Sanna, G. Minghetti, F. Demartin and M. Manassero, *Inorg. Chem., 28* (1989) 404.
[43] N.M. Hostie and R.F. Fenske, *Inorg. Chem., 22* (1983) 666.
[44] R. Cini, F.P. Fanizzi, P.F. Intini, L. Maresca and G. Natile, *J. Am. Chem. Soc., 115* (1993) 5123.
[45] J.G. Verkade and L.D. Quin, *Phosphorus-31 NMR Spectroscopy in Stereochemical Analysis, Organic Compounds and Metal Complexes*, VCH, Deerfield Beach, FL, 1987, p. 8.
[46] J.F. Nixon and A. Pidcock, in E.F. Mooney, *Annual Review of NMR Spectroscopy*, Vol. 2, Academic Press, London, 1969, p. 345.
[47] A.J. Gordon and R.A. Ford, *The Chemist's Companion: A Handbook of Practical Data, Techniques and References*, Wiley-Interscience, New York, 1972.
[48] J. Wesemann, P.G. Jones, D. Schomburg, L. Heuer and R. Schmutzler, *Chem. Ber., 125* (1992) 2187.
[49] G.M. Sheldrick, *SHELXTL PC, Vers. 4.2*, Siemens Analytical X-ray Instruments, Madison, WI, 1990.
[50] C. Mealli and D.M. Prosperio, *J. Chem. Edu., 167* (1990) 389.
[51] R. Hoffmann, *J. Chem. Phys., 39* (1963) 1397.
[52] R. Hoffmann and W.N. Lipscomb, *J. Chem. Phys., 36* (1962) 3179, 3489; *37* (1962) 2872.
[53] M.H. Sirretz and R.E. Weston, *J. Chem. Phys., 21* (1953) 898.
[54] T.A. Albright, R. Hoffmann, J.C. Thibeault and D.L. Thorn, *J. Am. Chem. Soc., 101* (1979) 3801.
[55] D.J. Schwartz and R. Andersen, *J. Am. Chem. Soc., 117* (1995) 4014.
[56] A. Modinos and P. Woodward, *J. Chem. Soc., Dalton Trans.*, (1975) 1516.
[57] C.W. Chan, T.F. Lai, C.M. Che and S.M. Peng, *J. Am. Chem. Soc., 115* (1993) 11245.
[58] W. Burger and J. Strahle, *Z. Anorg. Allg. Chem., 27* (1986) 539.
[59] R. Cini, F.P. Fanizzi, F.P. Intini and G. Natile, *J. Am. Chem. Soc., 113* (1991) 7805.
[60] L.A.M. Baxter, G.A. Healh, R.G. Raptis and A.C. Willis, *J. Am. Chem. Soc., 114* (1992) 6944.